Preprint typeset using LaTeX style emulateapj v. 21/08/00

THE ENERGY DEPENDENCE OF MILLISECOND OSCILLATIONS IN THERMONUCLEAR X-RAY BURSTS

Michael P. Muno,[1] Feryal Özel,[2] and Deepto Chakrabarty[1,3]

Submitted to ApJ.

ABSTRACT

We examine the energy-resolved pulse profiles of 51 flux oscillations observed during the decline of thermonuclear X-ray bursts from accreting weakly-magnetized neutron stars with the *Rossi X-ray Timing Explorer*. We find that the fractional rms amplitudes of the oscillations increase as a function of energy by 0.25% keV^{-1} to 0.9% keV^{-1} between $3-20$ keV, and are as large as 20% in the $13-20$ keV band. We also show that the pulses observed in the higher energy bands generally lag behind those in lower energy bands by 0.002 cycles keV^{-1} to 0.007 cycles keV^{-1} between $3-20$ keV. This amounts to total delays of 0.03–0.12 cycles between the lowest and highest energy bands, or time delays that range from 100–200 μs. We then model the oscillations as flux variations arising from temperature patterns on the surfaces of rapidly rotating neutron stars. In this framework, we find that the increase in the pulse amplitude with photon energy can be explained if the cooler regions on the neutron star emit in the lower energy bands, reducing the flux variations there. On the other hand, the Doppler shifts caused by the rapid rotation of the neutron star should cause the hard pulses to precede the soft pulses by about 0.05 cycles (100 μs), in contrast to the observations. This suggests that the photons originating from the stellar surface are reprocessed by a hot corona of electrons before they reach the observer.

1. INTRODUCTION

Thermonuclear bursts from accreting weakly-magnetized neutron stars provide an excellent opportunity to study emission originating from the stellar surface (see Lewin, van Paradijs, & Taam 1993 for a review). For instance, the unstable helium burning that produces the bursts may leave asymmetries in the surface brightness of the star that can be observed as pulsations at the stellar spin frequency (**?**, e.g.,)]fw82,str97. Indeed, oscillations that are apparently produced by bright regions on rapidly rotating neutron stars now have been observed during bursts from ten neutron star low-mass X-ray binaries (LMXBs) with the *Rossi X-ray Timing Explorer* (**?**, *RXTE*; see)for a review]str01. Their frequencies range between 270–620 Hz (Muno et al. 2002a), which are consistent with the assumption that these LMXBs are the progenitors of recycled millisecond radio pulsars (Alpar et al. 1982; Radhakrishnan & Srinivasan 1982). Most importantly, after a small frequency drift is accounted for, the oscillations are extremely coherent. The oscillations have quality factors $Q = \nu/\Delta\nu > 1000$ during individual bursts (Strohmayer et al. 1996; Strohmayer & Markwardt 1999, 2002; but see Muno et al. 2002a), and they appear at frequencies that are stable to a few parts in 1000 in bursts observed over several years from any given source (Strohmayer et al. 1998b; Giles et al. 2002; Muno et al. 2002a). The stability and coherence of these oscillations provides compelling evidence that they originate from brightness patterns on rotating neutron stars.

Burst oscillations therefore allow one to study a range of questions, including the physics of nuclear burning on the stellar surface, the effects of gravitational self-lensing by the neutron star, and the equation of state of dense nuclear matter. The most constraining data so far have come from the amplitudes and the profiles of the oscillations. The fractional rms amplitudes of the oscillations can be as large as 50% during the first second of a burst (Strohmayer et al. 1998a). If the oscillations result from two antipodal bright regions on the surface, as has been proposed based upon both observational and theoretical considerations (Miller, Lamb, & Psaltis 1998; Miller 1999), then amplitudes this large can only be produced if the neutron star is larger than $R/R_{\rm Sch} = 3.1$ (Miller & Lamb 1998; Nath, Strohmayer, & Swank 2002), where $R_{\rm Sch}$ is the Schwarzschild radius. Moreover, the profiles of the oscillations are nearly perfectly sinusoidal — the amplitudes of the harmonic components are less than 0.5% of those of the main signals. This suggests that the patterns forming on the stellar surfaces are either highly symmetric or restricted to near the rotational poles (Muno, Özel, & Chakrabarty 2002b).

The surface velocity of the neutron star ($\approx 0.1c$ for a 10 km star spinning at 500 Hz) can be measured from variations in the amplitude and phase of the oscillations as a function of energy, which would provide another constraint on the stellar radius. The amplitudes of the oscillations should increase as a function of energy because Doppler shifts cause the Wien tail of the spectral distribution to move in and out of the highest energy bands (Miller & Lamb 1998). However, the amplitudes will also be set by the surface temperature distribution, since a finite surface temperature produces a constant background against which a hot region is less distinct at low energies (Page 1995). The relative phases of the waveforms as a function of energy, on the other hand, are affected only by the Doppler shifts of the tail of the spectrum, which move the

[1] Department of Physics and Center for Space Research, Massachusetts Institute of Technology, Cambridge, MA 02139, muno@space.mit.edu, deepto@space.mit.edu

[2] Hubble Fellow; Institute for Advanced Study, Einstein Dr., Princeton, NJ 08540

[3] Alfred P. Sloan Research Fellow

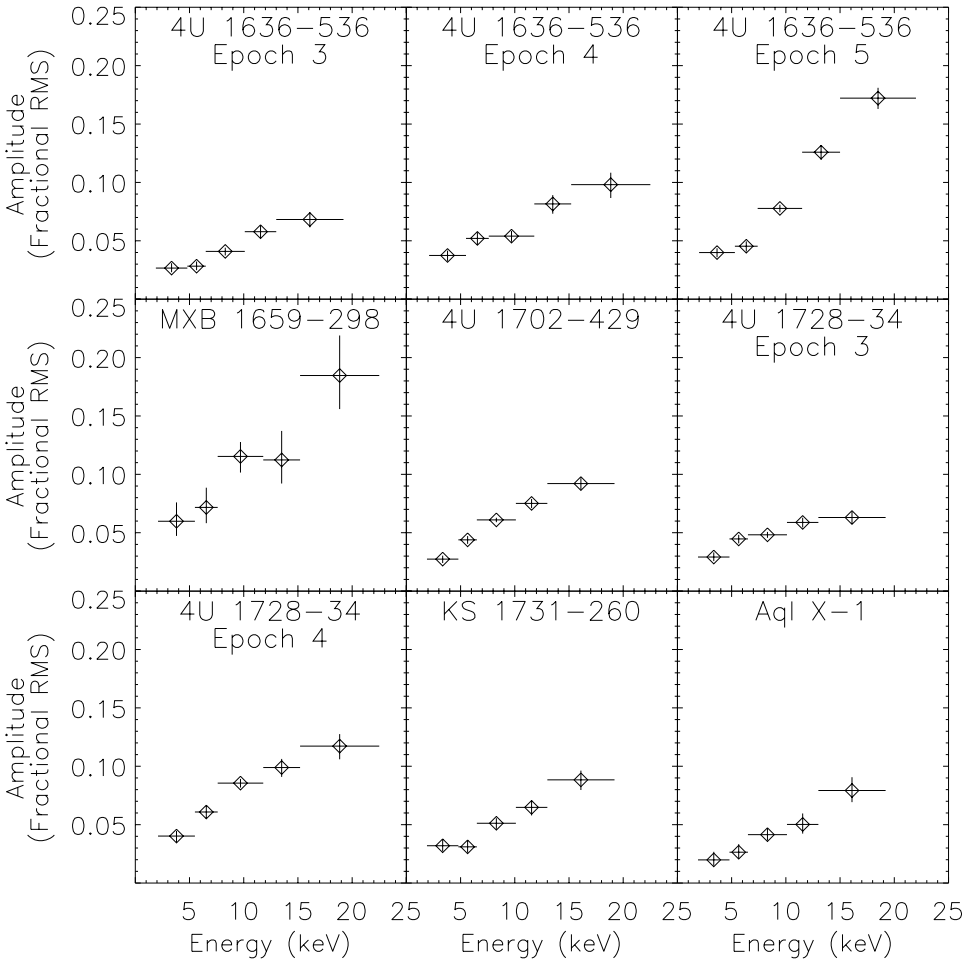

FIG. 1.— The energy dependence of the amplitudes of the averaged oscillation profiles from six sources. For each source, oscillations were only averaged for a single epoch during which the gain of the PCA was relatively constant. In all cases, the amplitudes increase significantly as a function of the photon energy.

peak of the high-energy pulse to an earlier phase (Braje, Romani, & Rauche 2000; note that Doppler beaming and photon arrival time delays also shift the overall phase of the entire pulse). Evidence that the hard pulse leads the soft has been reported in a burst oscillation from Aql X-1 by Ford (1999), although further studies question whether this is due to rotational motion (Fox 2000).

In this paper, we present a study of the amplitudes and phases of burst oscillations as a function of photon energy. In Section 2 we analyze the energy-resolved waveforms of 59 oscillations observed with the Proportional Counter Array (PCA) on *RXTE*. In Section 3, we present theoretical waveforms produced from the models of Muno et al. (2002b), taking into account the response of the PCA to facilitate comparison with the data. We consider several simple temperature distributions on the neutron star. In Section 4, we explore whether we can measure Doppler effects in the observed waveforms.

2. OBSERVED WAVEFORMS

As part of an ongoing study of thermonuclear bursts observed with the *RXTE* Proportional Counter Array (**?**, PCA;)]jah96, we identified 68 X-ray bursts containing millisecond oscillations in data from eight sources that were in the public domain as of September 2001 (Muno et al. 2002a). The PCA is composed of five gas-filled proportional counter units (PCUs) that are sensitive to X-rays between 2.5–60 keV with an energy resolution of about 15%. Between 2 and 5 PCUs were active during the observations in our sample. Each PCU has an effective area of 1200 cm^2 and is capable of recording photon arrival times with microsecond time resolution. For most of the observations, data with both 2^{-13} s (122 μs) time resolution and between 8–64 energy channels were recorded on an event-by-event basis, and were used to study the profiles of the oscillations.

We first modeled the frequency evolution of the oscillations observed in the entire PCA bandpass using a phase connection technique similar to that used in pulsar timing (Manchester & Taylor 1977; Muno et al. 2002a). To

implement this technique, we folded the data in short intervals (0.25–0.5 s) using a trial phase model, which was then refined through a least χ^2 fit to the residuals. This provides excellent frequency resolution and a statistical measure of how well the model reproduces the data. We have previously used the resulting phase models to study the frequency evolution, amplitudes, and profiles of the burst oscillations (Muno et al. 2002a; Muno et al. 2002b).

We then applied the best-fit phase models to produce folded profiles in 7 energy channels. Since the gains of the proportional counters have been changed several times during the mission, the energies corresponding to the detector channels vary. Data with sufficient energy and time resolution were only used to record burst oscillations in gain epochs 3 (1996 April 15 through 1999 March 22), 4 (1999 March 22 through 2000 May 13), and 5 (2000 May 13 to present). We were unable to choose detector channels with identical energy boundaries in different gain epochs, since the high time resolution data were usually taken with too few energy channels. Therefore, we defined the energy boundaries by detector channels 5, 13, 18, 28, 36, and 53. These boundaries roughly correspond to <2, 5, 7, 10, 13, and >20 keV during gain epoch 3 (see also Table 1). The low (< 2 keV) and high (> 20 keV) energy channels generally were dominated by background events, and were therefore ignored during our analysis. We found that 51 oscillation trains from 6 sources were sampled with adequate time and energy resolution for this study. The sources, oscillation frequencies, and numbers of oscillations examined are listed in Table 2.

We note that the energy-resolved data that we used (Table 2) contained up to 30% fewer counts than the profiles created for a single energy channel in Muno et al. (2002b). This is because the *RXTE* data buffers could only record energy-resolved data for a fraction of each second before they were filled during the brightest segments of many bursts. Other modes designed specifically to record bursts were available for producing the frequency models (so-called burst-catcher modes), but sacrificed energy resolution in favor of high time resolution. The burst-catcher modes were not used to produce energy-resolved waveforms.

We measured the amplitudes of the oscillations as a function of energy by computing a Fourier power spectrum of the folded profiles in units of total counts per phase bin. We normalized the power according to Leahy et al. (1983), so that the fractional rms amplitude at any multiple of the oscillation frequency is

$$A_n = \left(\frac{P_n}{I_\gamma}\right)^{1/2} \frac{I_\gamma}{I_\gamma - B_\gamma}, \quad (1)$$

where P_n is the power at the nth bin of the Fourier spectrum, I_γ is the total number of counts in the profile, and B_γ is the estimated number of background counts in the profile. The background was taken to be the persistent emission during the 15 s prior to the burst. This equation is valid so long as the phase and frequency of the oscillation is known, as it is by design for our folded profiles. Uncertainties and upper limits on the amplitudes are computed taking into account the distribution of powers from Poisson noise in the spectrum, using the algorithm in the Appendix of Vaughan et al. (1994). We measured the phases of the oscillations by linear least-squares fits of sinusoids to the folded profiles. The uncertainties on the phases were determined from the diagonal values of the covariance matrices that were derived as part of the least-squares algorithm (Press et al. 1992).

We also summed the energy-resolved profiles for all of the oscillations that occurred during an individual gain epoch from each source (Table 2). Although the gain of the PCA drifted even during a single epoch, we confirmed that the drift was not large enough to affect the summed profiles. We did so by folding a set of simulated profiles (see Section 3) through different responses generated by the FTOOL[4] `pcarsp` that spanned gain epoch 3, measuring the amplitude and phase of each individual oscillation, and comparing it to those of the summed profile. The values were identical to within less than 1%.

2.1. *Amplitudes as a Function of Energy*

First, in order to determine whether the oscillation amplitudes in individual bursts change significantly as a function of photon energy, we calculated the χ^2 statistic under the assumption that the amplitudes are constant:

$$\chi^2 = \sum \left(\frac{A_i - \bar{A}_i}{\sigma_{A_i}}\right)^2, \quad (2)$$

where A_i is the fractional rms amplitude in each energy band, $\bar{A}_i$ is the mean amplitude, and σ_{A_i} is the uncertainty derived according to the method of Vaughan et al. (1994). We find that 34 of 51 oscillations are inconsistent with a constant amplitude as a function of energy at the 90% confidence level. The remaining oscillations that appear to have constant amplitudes typically have fewer counts in the folded profile: the mean number of counts in a folded profile is 5.5×10^4, while those with constant amplitudes have on average 3.5×10^4 counts.

To quantify how the amplitude varies with energy in these oscillations, we fit them with a linear function using a least-squares technique. A linear fit is only a crude approximation to the functional form expected from a hot region on a rotating neutron star (see Section 3), but it is adequate for making simple quantitative comparisons between our observational and theoretical results, given the limited statistics in most of our measurements. We found that 28 oscillations were consistent with a linear increase in amplitude as a function of energy. The average of the best-fit slopes for these oscillations was 0.8% keV^{-1}. The smallest total detectable increase in amplitude was about 2% between the 2 keV and 20 keV bands, while the increase was as large as 30% in several oscillations from 4U 1636−536 and 4U 1702−429. Only 6 oscillations were inconsistent with both constant amplitudes and linear trends. Two of these (occurring on 1996 December 21 17:30:34 and 1999 June 21 19:13:02 from 4U 1636−536, where these and all subsequent times are in Barycentric Dynamical Time) exhibit random variations in amplitude, while the remaining four (occurring on 2000 June 15 05:13:02 and 2000 August 9 09:00:34 from 4U 1636−536, and on 1997 September 20 10:08:27 and 1999 August 19 12:13:22 from 4U 1728−34) show deviations from a linear trend that are consistent with the functional form expected from a hot region on a rotating neutron star (see Section 3).

[4] `http://heasarc.gsfc.nasa.gov/docs/software/ftools/`

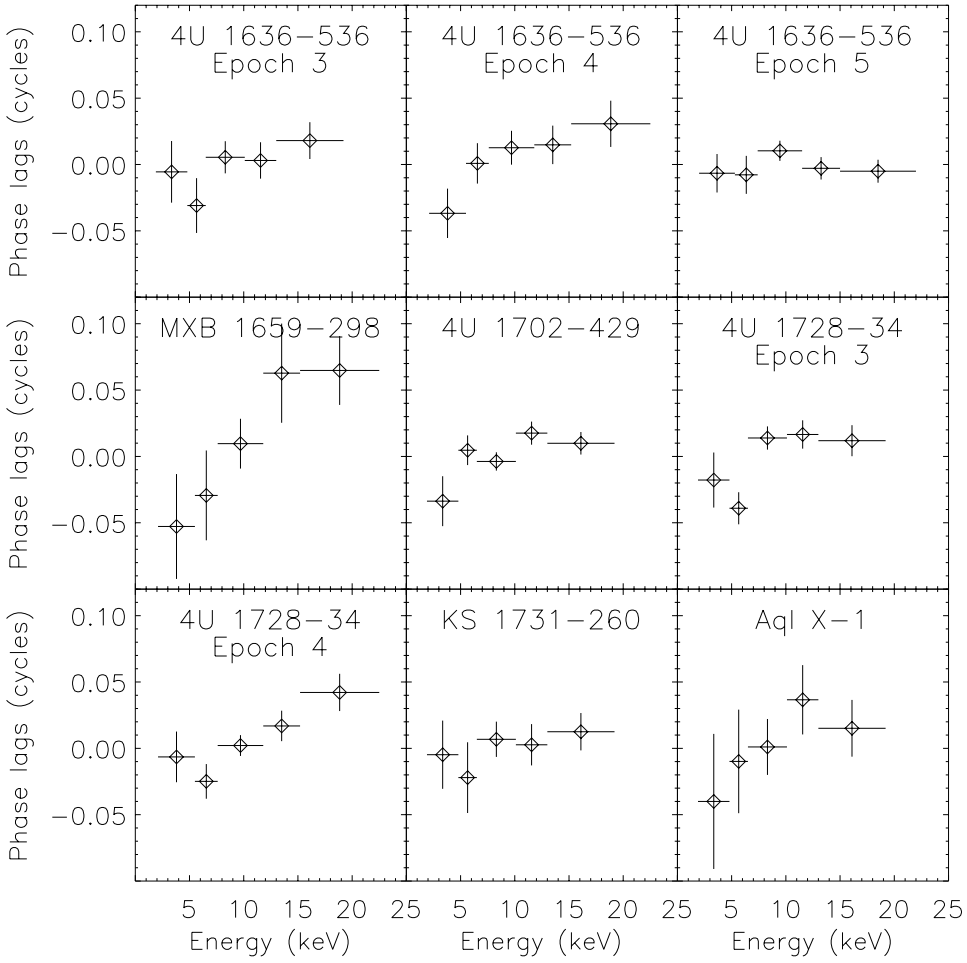

FIG. 2.— The energy dependence of the phases of the averaged oscillation profiles from six sources (compare Figure 1). Phase zero is defined by the profile in the total PCA bandpass. A positive value of the phase lag indicates that the profile in that energy range arrives later than the average profile.

We then performed the same analysis for 9 summed pulse profiles from 6 sources. We list the results in Table 3, and we display the amplitude as a function of energy in Figure 1. The amplitudes from all of the summed profiles increase as a function of energy with $> 99.9\%$ confidence. In most cases, the increase is consistent with linear functions with slopes between 0.5–0.8% keV^{-1}. This translates to a total increase in amplitude from 5–16% between 2–20 keV. Only the oscillations from 4U 1636−536 in gain epoch 5 are inconsistent with a linear trend. These have a higher amplitude in the 2–5 keV band than would be expected from extrapolating the trend at higher energies (Fig. 1), but are still roughly consistent with the functional form expected from a hot spot.

2.2. *Phase as a Function of Energy*

We then examined the relative phases of the oscillations as a function of energy. The reference phases were taken to be those of the oscillations in the total 2–60 keV bandpass. An increasing value of the phase lag indicates that the pulse seen at high energies arrives later than (lags) that at low energies. Of the individual oscillation trains, we find that only 13 exhibit phases that vary as a function of energy at the 90% confidence level. Of these 13 oscillations, 6 appear to change in phase with a slope of $-0.005(3)$ to $0.019(5)$ cycles keV^{-1} (1999 April 29 01:49:24 from 4U 1636−536; 1999 April 10 09:54:12 from MXB 1659−298; 1999 February 22 04:54:01 from 4U 1702−429; 1999 August 19 15:50:57 from 4U 1728−34; and 1996 July 14 04:23:45 and 1999 February 26 17:10:56 from KS 1731−260). Seven oscillations are not well-fit by linear trends, but exhibit random variations in phase as a function of energy (2000 August 9 01:22:23 and 09:00:34 from 4U 1636−536; 1997 July 26 09:09:11 from 4U 1702−429; 1997 September 21 18:10:31, 1997 September 27 11:17:45, 1999 January 31 21:56:41, and 1999 August 19 12:13:22 from 4U 1728−34). The weighted average of the phase lag for the 44 oscillations that can be adequately fit with a linear trend is $0.0024(5)$ cycles keV^{-1}.

In Figure 2 we plot the phase as a function of energy

for 9 summed profiles from 6 sources, and in Table 4 we compile the results. Applying the χ^2 statistic to the data, we find that the phase varies as a function of energy at the 90% confidence level in 5 of the 9 oscillations. In 4 of these 5 oscillations, the phases are consistent with a linear increase as a function of energy with a slope of between 0.002(1) and 0.007(3) cycles keV^{-1}. Thus, the pulses at 20 keV lag behind those at 2 keV by 0.04-0.14 cycles, which translates to time delays of 100 μs (4U 1702−429) to 200 μs (MXB 1659−298). The summed oscillation from 4U 1728−34 in gain epoch 3 appears to exhibit random variations in phase as a function of energy, as is evident in Figure 2.

We note that our sample includes the oscillation from Aql X-1 in which Ford (1999) reported that the pulse at high energies *precedes* that at low energies in the last half of the oscillation train. We find that these soft lags are significant only in the interval that was searched, while earlier the oscillation exhibited hard lags (**?**, see also)]fox00. Over the entire burst, the soft and hard lags cancelled, yielding no net delay between hard and soft photons. We searched for similar changes in the energy dependence of the phases of other oscillations by dividing the oscillations into two intervals containing an equal number of counts. We did not find any other significant examples of phase lags switching from positive to negative.

3. MODEL PROFILES

In this section, we examine how the rotation of the neutron star affects the energy dependence of the burst oscillations. To that end, we produce theoretical energy-resolved light curves from circular hot spots on a rotating neutron star. We use the techniques outlined by Pechenick, Ftaclas, & Cohen (1983), Braje et al. (2000), and Weinberg, Miller, & Lamb (2001). The amplitudes and profiles of our theoretical oscillations in the entire PCA bandpass (2–60 keV) are discussed extensively in Muno et al. (2002b).

The energy spectra observed during bursts can adequately be modeled as blackbody emission with a temperature kT_∞. Therefore, we use the same spectral distribution to describe the emission from the neutron star's surface. The angular dependence of the emission is described by a Hopf function (Chandrasekhar 1960), which is appropriate for the scattering-dominated atmosphere present during a burst (**?**, e.g.,)]mad91. Photons are propagated to the observer through a Schwarzschild metric about a compact object with compactness $p \equiv R/2M$. Corrections to the metric due to the unknown density structure of the neutron star should be of order a few percent (**?**, e.g.,)]brr00, which is of the same magnitude as the measurement uncertainties in the observed waveforms. We assume that the neutron star has a mass of 1.4 $M_\odot$, and denote its rotation frequency with Ω.

We consider one single and two antipodal circular bright regions with a constant temperature, with the rest of the surface taken to emit at a lower temperature. The circular hot region(s) are taken to have angular radius ρ and to be centered at an angle α from the rotational axis of the neutron star. The angle between the line-of-sight of the observer and the spin axis of the neutron star is denoted by β. In total, our simulations include seven parameters that can affect the energy dependence of the oscillations: the compactness and the spin frequency of the neutron star; the number, size, position, and temperature contrast of the hot regions; and the viewing angle of the observer.

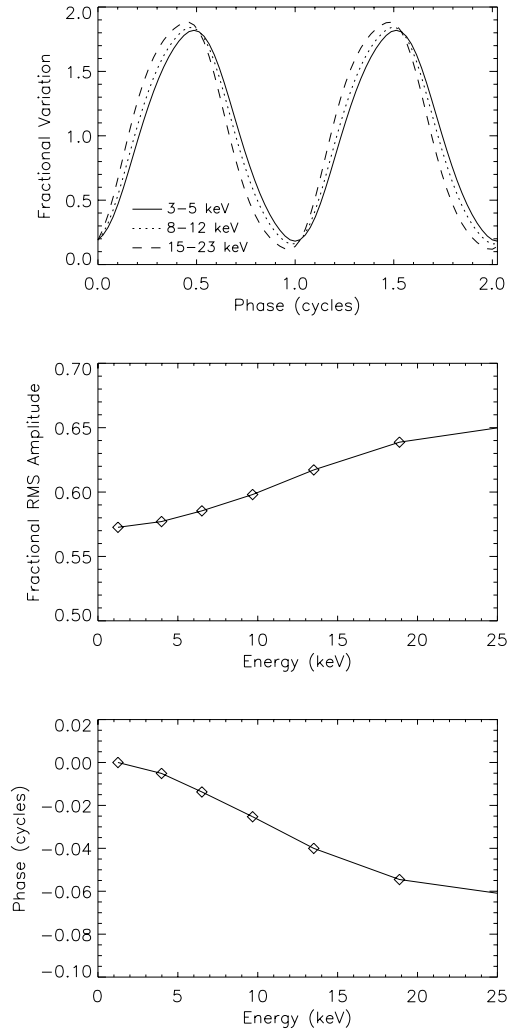

FIG. 3.— Illustration of the energy dependence of the oscillation profiles from our theoretical models of a bright region on a rotating neutron star. We model a 1.4 $M_\odot$ neutron star with a radius of 10 km ($p = 2.5$) spinning at $\Omega = 600$ Hz. The bright region has a size $\rho = 90°$, is located at $\alpha = 90°$, and is viewed from $\beta = 90°$. The response of the *RXTE* PCA was accounted for in computing the model profiles. The Doppler and time delay effects introduced by the rotation of the star cause the amplitude of the oscillation increases by 6% between 1–20 keV, while the phase of the oscillation at 20 keV precedes that at 1 keV by 0.055 cycles.

For each set of parameters, we produce light curves in 40 phase bins and in 64 energy bins logarithmically spaced between 0.01–25 keV. The observed spectrum is simply a sum of blackbodies whose temperatures are multiplied by Doppler factors; therefore, the signal from a bright region of arbitrary temperature can be obtained by rescaling from a calculation with $kT = 1$ keV. For each phase, the resulting spectra are folded through a fiducial PCA response matrix, which we generated for PCU 2 during December 1999 (gain epoch 3), in order to obtain predicted light curves that can be compared directly to the observations. We analyze these light curves in the seven energy chan-

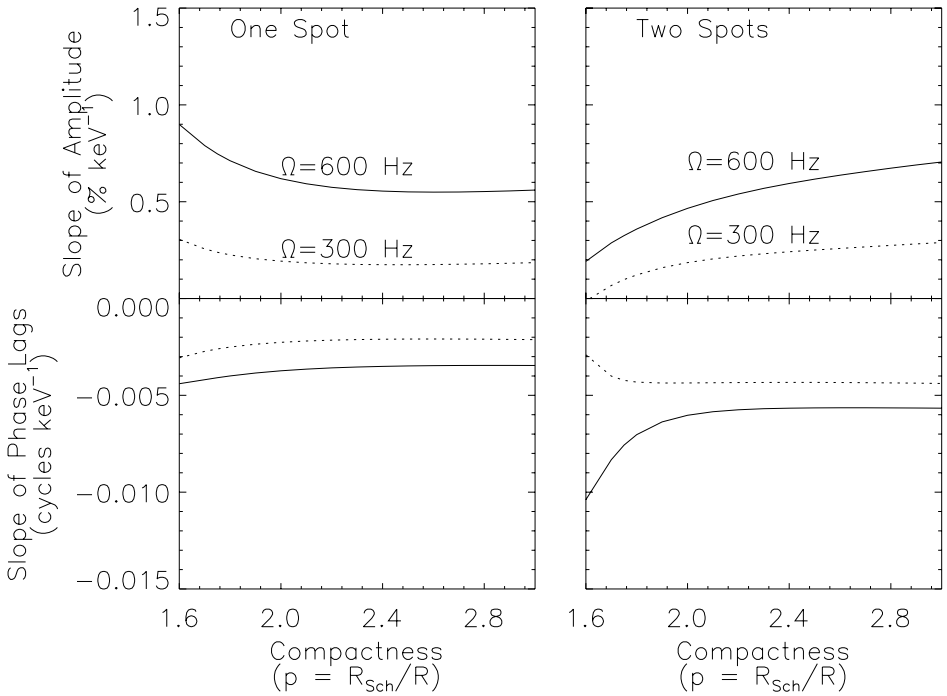

FIG. 4.— Effects of the compactness $p = R/R_{\rm Sch}$ on the predicted slopes of the amplitude and phase as a function of energy, for two values of the spin Ω, and considering both one and two bright regions. Here, $\alpha = \beta = 90°$ and $\rho = 60°$.

nels used in Section 2, using the same Fourier techniques to measure the amplitudes of the oscillations, and a least-squares fit to measure the phases. The amplitudes and phases we report are measured for the Fourier component at the spin frequency of the star when one hot spot is modeled, and at twice the spin frequency when two antipodal spots are modeled.

3.1. *Energy Dependence of the Oscillations*

In Figure 3 we show the effects of the rotation of the neutron star on the energy-dependent profiles of the oscillations (*top panel*), and on the corresponding amplitudes (*middle panel*) and phases (*bottom panel*) from a single circular bright region of temperature $kT_\infty = 2.3$ keV at infinity. Here, the bright region covers half the star ($\rho = 90°$), is centered at the equator ($\alpha = 90°$), and is viewed along the equator ($\beta = 90°$). The star has a compactness $p = 2.5$ and spin $\Omega = 600$ Hz.

Stellar rotation introduces two main effects: the fractional amplitudes are larger in the higher energy bands, and the pulses at higher energies precede those at lower energies (*top panel* of Fig. 3). Both effects occur because the spectrum is steepest at high energies (≈ 20 keV), so that a slight Doppler shift in the apparent photon energy results in a significant change in the flux received. This not only yields a larger fractional amplitude at ≈ 20 keV, but also causes the hard pulse to peak as the spot rotates toward the observer, before the observer sees the largest solid angle from the spot at lower energies.

We quantify the energy dependence in Figure 3 in the same manner as in Section 2, by measuring the fractional rms amplitudes (*middle panel*) and phases (*bottom panel*) of the oscillations in each energy band. We perform a linear least-squares fit to the middle 5 energy channels (2–20 keV) from our simulations to determine the slopes of the amplitudes and phases as a function of energy. For the example in Figure 3, the amplitude increases by approximately 0.4% keV^{-1}, while the phases of the higher-energy photons lead those at lower-energy by about 0.003 cycles keV^{-1}.

In Figure 4 we display how the amplitudes (*top panels*) and phases (*bottom panels*) of the oscillations depend on the spin and compactness of the neutron star. The left panels illustrate the dependencies for the case of a single bright region, while the right panels illustrate the case of two antipodal regions. The bright regions have a constant temperature $kT_\infty = 2.3$ keV at infinity and a size $\rho = 60°$, are located at $\alpha = 90°$, and are viewed along $\beta = 90°$. The rest of the star is assumed to be dark.

We find that the energy dependence of both the amplitudes and phases are considerably stronger when the neutron star is spinning rapidly ($\Omega = 600$ Hz; solid line), simply because the Doppler shifts are more pronounced. However, the dependence on compactness in Figure 4 is more complex. At larger compactness, $p > 2.5$, the magnitudes of the amplitude increase are very similar for one or two bright regions, although the phase lags are about 75% larger from two spots. At small compactness ($p < 1.7$), the energy dependence of the pulse profiles from one and two bright regions behave quite differently, because the bright region is strongly lensed on the opposite side of the star from the observer (Pechenick et al. 1983). The lensing causes the relative phases at which (*i*) the observer sees the largest solid angle from the emitting region and (*ii*) the Doppler effects are strongest to differ for the Fourier components at the spin frequency and its harmonic. We use $p = 2.5$ throughout the rest of our simulations, which corresponds to a 1.4 $M_\odot$ star with a 10 km radius.

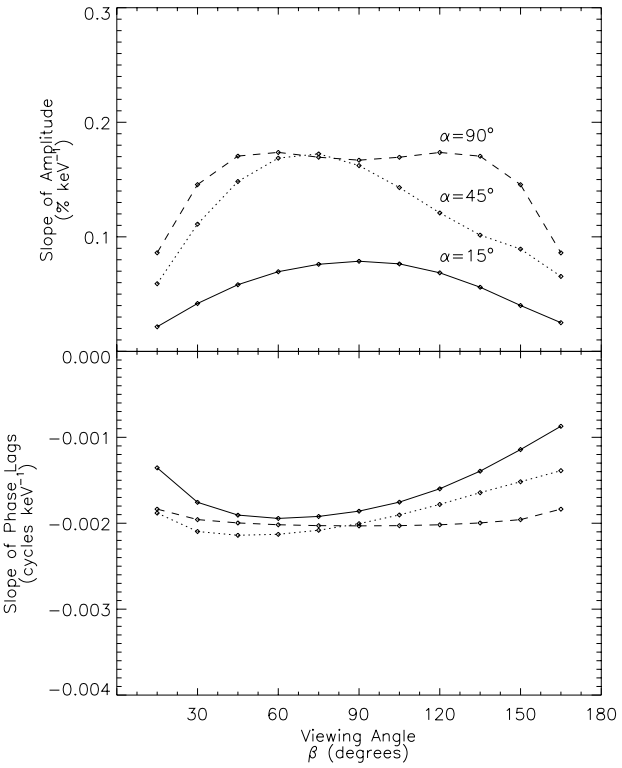

FIG. 5.— Effects of changing the viewing angle β (x-axis) and the position of the bright region α (solid, dotted, and dashed lines) on the slopes of the amplitude and phase as a function of energy. A single bright region with $\rho = 60°$ was modeled, on a $p = 2.5$ neutron star with $\Omega = 300$ Hz.

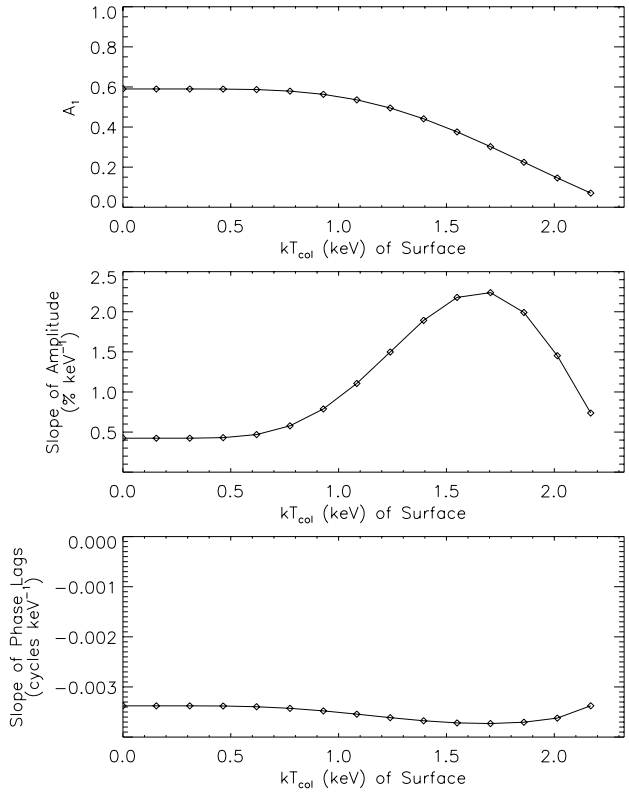

FIG. 6.— Effects of changing the temperature of the rest of the neutron star, while keeping the bright region at a constant temperature of $kT_\infty = 2.3$ keV as observed at infinity. We have taken $\rho = \alpha = \beta = 90°$, $\Omega = 600$ Hz, and $p = 2.5$. *Top panel*: The amplitude of the oscillation in the full PCA bandpass decreases monotonically as the temperature of the surface approaches that of the bright region. *Center panel*: The slope of the amplitude as a function of energy reaches a maximum when the rest of the star emits within the PCA bandpass, such that at low energies the oscillation is muted by a phase-independent background flux, while at high energies the emission is only observed from the hot region. *Bottom panel*: Varying the temperature contrast only slightly affects the slope of the phase as a function of energy.

We also find that as the size ρ of the bright regions increases, the slope of the amplitude as a function of energy decreases monotonically. This is due to the facts that (*i*) the amplitudes of the oscillations decrease in general, and (*ii*) points on the bright regions have a range of velocities with respect to the observer, which damps the magnitude of Doppler effects. The phase lags do not vary as a function of the size of the bright regions, because the phase of the peak of the pulse is not changed by the effective background provided by the regions of a larger spot that are not Doppler-shifted.

In Figure 5, we illustrate the effects of changing the viewing angle (β) and position (α) of one bright region on the energy dependence of the amplitudes and phases. Here we take $\rho = 90°$ and $kT_\infty = 2.3$ keV, and assume that the rest of the star is dark. The neutron star has $p = 2.5$ and $\Omega = 300$ Hz. We find that the slopes of both the phases and amplitudes generally decrease in magnitude as the bright region or the observer are moved closer to the poles, because the relative velocity of the spot and the observer decreases. The slope of the fractional amplitude as a function of energy decreases more rapidly because the amplitude of the oscillation decreases, just as occurs when the size of the bright region is increased.

As the temperature of the bright regions increases, the slopes of the phase lags and amplitudes flatten very slightly, because the peak of the energy spectrum moves to higher energies. However, if the rest of the neutron star also emits within the bandpass of the detector, the energy dependence of the oscillations can become quite dramatic, as we illustrate in Figure 6. The slope induced by the temperature contrast is more than five times larger than that produced by Doppler motion alone (i.e., when $kT_{\rm col} = 0$). At low energies, the cooler regions on the neutron star contribute a constant background flux to the oscillations, decreasing their fractional amplitude. At high energies, where the cool regions of the neutron star contribute little flux, the amplitude of an oscillation is similar to that which one would see if the neutron star were dark. The largest slope attainable increases as the size of the hot region ρ decreases. On the other hand, the phases of the oscillations are weakly dependent on the temperature contrast from the neutron star, for the same reasons that the phases are not affected greatly by varying the sizes and positions of the bright regions. Thus, the phase lags provide the best measure of the apparent velocity of the bright region.

4. DISCUSSION

4.1. *Amplitude as a Function of Energy*

In all of the burst oscillations, we find that the observed increase in amplitude as a function of photon energy is about 50% larger than is expected from Doppler effects alone. In the sources with $\approx$ 600 Hz oscillations, 4U 1636−536 and MXB 1659−298, the amplitude increases by up to 0.8–0.9 % keV^{-1} (see Table 3 and Fig. 1), while a single bright region on a star spinning at 600 Hz can yield a 0.6 % keV^{-1} increase, and two antipodal regions on a star with $\Omega = 300$ Hz can give rise to a 0.3% keV^{-1} increase (Fig. 4). Similarly, the amplitudes of the $\approx$ 300 Hz oscillations from 4U 1702−429 and 4U 1728−34 increase by 0.5–0.6% keV^{-1}, compared to the 0.2% keV^{-1} increase that might be expected from a bright region on a neutron star with $\Omega = 300$ Hz. These differences are significant, as our uncertainties on the measured slopes are less than 0.01% keV^{-1}.

It is therefore likely that the observed increase in amplitude as a function of energy occurs because the rest of the neutron star also emits in the the lower energy bands of the PCA (Fig. 6), thus reducing the flux variations at these energies. To estimate the magnitude of the temperature contrast that could produce these oscillations, we use the constraints on the sizes and locations of bright regions that are consistent with the observed oscillation profiles from Muno et al. (2002b). Using the lack of harmonic signals, Muno et al. (2002b) show that the pulsations can only be produced by (*i*) a single bright region that covers nearly half the neutron star ($\rho \approx 90^\circ$), (*ii*) a single bright region that forms within $\alpha < 20^\circ$ from the rotational pole, or (*iii*) two antipodal bright regions that form within a few degrees of the rotational equator $\alpha \approx 90^\circ$.

A single $\rho = 90^\circ$ bright region (case *i*) would produce oscillations with an rms amplitude of 55% if the rest of the star were dark (Fig. 6, *top panel*). Since the observed amplitudes of the oscillations are 3–5 times smaller even in the highest energy band, it is necessary to assume that the other half of the neutron star also emits, but at a lower temperature, in order to reproduce the observed oscillations. A temperature contrast of about 0.15 keV between the two hemispheres would produce oscillations with an amplitude of 5–10% in the full PCA bandpass (Table 1 in Muno et al. 2002b) and an amplitude increase of 0.7% keV^{-1} (Table 3). In cases (*ii*) and (*iii*), on the other hand, the sizes of the spots are not well-constrained, and thus one can reproduce the observed amplitudes with either small hot spots and a small temperature contrast, or with large bright regions and a larger temperature contrast (compare Fig. 6 with Fig. 4 in Muno et al. 2002b).

Finally, we note that the increases in the amplitudes of the burst oscillations as a function of energy are not a generic feature of all coherent pulsations from LMXBs. The amplitudes of the persistent pulsations from the accretion-powered millisecond X-ray pulsars SAX J1808.4−3658 and XTE J0929−314 actually decrease in amplitude between 2–10 keV. This suggests that a different emission mechanism or geometry may play a role in the generation of pulsations in these two classes of LMXBs.

4.2. *Phase as a Function of Energy*

As can be seen from Table 4 and Figure 2, the phase lags observed from all of the combined pulse profiles are consistent either with being constant as a function of energy, or with increasing slightly such that the hard pulse arrives after the soft pulse. Only one set of oscillations, observed from 4U 1636−536 in gain epoch 5, is consistent with a negative slope, and in this case an energy-independent phase is also an acceptable fit. The magnitudes of the phase lags are on order 0.5–0.1 cycles between 2–20 keV, which translates to a time delay of ≈ 150 μs for spin frequencies between 300–600 Hz. Thus, the signs of the observed phase lags are generally opposite the negative phase lags that are expected from Doppler effects, although the magnitudes of the lags are comparable. In contrast, the sign of the phase lags observed from the accretion-powered millisecond X-ray pulsars SAX J1808.4−3658 and XTE J0929−314 are consistent with those that would be expected from Doppler effects, as the pulse at 10 keV is observed to precede that at 2 keV by 200–700 μs (Cui, Morgan, & Titarchuk 1998; Galloway et al. 2002).

To understand the sign of the lags, we consider whether interactions between photons from the neutron star and material (*i*) in the accretion disk or (*ii*) in a hot corona could modify the energy dependence of the phases of the oscillations. In the first case, photons that get scattered by the accretion disk can acquire a Doppler shift from the motion of the orbiting material. However, since the disk is most likely to rotate in the same direction as the neutron star, the soft pulse would lag behind the hard (Sazonov & Sunyaev 2001), which is still inconsistent with the data. In the second case, a corona of hot electrons could induce hard phase lags if they inverse-Compton scatter photons from the neutron star to higher energies (**?**, e.g.,)]mil95. Indeed, the hard X-rays (> 10 keV) observed between bursts from neutron star LMXBs are thought to originate from such a corona (**?**, e.g.,)]bar00. It is not clear whether such a corona also exists during X-ray bursts, so evidence for it must be sought via simultaneous modeling of the burst spectra and the oscillation profiles. We also note that a hot corona of electrons could reduce the harmonic content of the oscillation profiles (**?**, e.g.,)]mil00,moc02.

5. CONCLUSIONS

We have examined the energy-dependence in the amplitudes and phases of a sample of 51 burst oscillations using data from the *RXTE* PCA (Table 2). We found that the fractional rms amplitudes of the oscillations increase as a function of energy by 0.25% keV^{-1} to 0.9% keV^{-1} between 3–20 keV (Fig. 1 and Table 3). We then modeled the oscillations as flux variations arising from temperature patterns on the surfaces of rapidly rotating neutron stars, and calculated the Doppler effects on the energy-resolved light curves. Comparing the models with the data, we found that the observed slope of the energy dependence is generally larger than would be expected from Doppler effects alone (Fig. 3). However, it can be reproduced by assuming that cooler regions of the neutron star also emit in the low energy bands of the PCA (Fig. 6).

We also found that the high-energy pulses generally lag behind the low-energy pulses in the observed light curves by 0.002(1) cycles rad^{-1} to 0.007(3) cycles rad^{-1} between

3–20 keV (Fig. 2 and Table 4). In contrast, Doppler effects should cause the high-energy pulses to precede the soft pulses by 0.003 cycles keV^{-1} (Fig. 3). Hard lags like those observed could conceivably be produced if the signals from the surfaces of these neutron stars are re-processed by scattering in a hot corona of electrons. However, it is not clear whether such a corona exists during the declines of the thermonuclear bursts that produce these oscillations. Further observational and theoretical study is warranted to address this issue.

We thank Dimitrios Psaltis for helpful discussions, and Duncan Galloway, Pavlin Savov, and Derek Fox for important contributions to the data analysis underlying this work. M.M. and D.C. were supported in part by NASA, under contract NAS 5-30612 and grant NAG 5-9184. F.Ö. acknowledges support by NASA through Hubble Fellowship grant HF-01156 from the Space Telescope Science Institute, which is operated by the Association of Universities for Research in Astronomy, Inc., under NASA contract NAS 5-26555.

REFERENCES

Alpar, M. A., Cheng, A. F., Ruderman, M. A., & Shaham, J. 1982, Nature, 300, 728
Barret, D., Olive, J. F., Boirin, L., Done, C., Skinner, G. K., & Grindlay, J. E. 2000, ApJ, 533, 329
Bildsten, L. 1995, ApJ, 438, 852
Bildsten, L. 1998, ApJ, 501, L89
Braje, T. M., Romani, R. W., & Rauch, K. P. 2000, ApJ, 531, 447
Chandrasekhar, S. 1960, *Radiative Transfer* (Dover)
Cui, W., Morgan, E. H., & Titarchuk, L. G. 1998, 504, L27
Ford, E. C. 1999, ApJ, 519, L73
Fox, D. W. 2001, PhD thesis, MIT
Fryxell, B. A. & Woosley, S. E. 1982, ApJ, 261, 332
Galloway, D. K., Chakrabarty, D., Morgan, E. H., & Remillard, R. A. 2002, ApJ, 576, L137
Giles, A. B., Hill, K. M., Strohmayer, T. E., & Cummings, N. 2002, ApJ, 568, 279
Jahoda, K., Swank, J. H., Giles, A. B., Stark, M. J., Strohmayer, T., Zhang, W., & Morgan, E. H. 1996, SPIE, 2808, 59
Leahy, D. A., Darbro, W., Elsner, R. F., Weisskopf, M. C., Sutherland, P. G., Kahn, S., & Grindlay, J. E. 1983, ApJ, 266, 160
Madej, J. 1991, ApJ, 376, 161
Manchester, R. N., & Taylor, J. H. 1977, Pulsars(San Francisco: W. H. Freeman and Co.)
Miller, M. C. 1995, ApJ, 441, 770
Miller, M. C. 1999, ApJ, 515, L77
Miller, M. C. 2000, ApJ, 537, 342
Miller, M. C. & Lamb, F. K. 1998, ApJ, 499, L37
Miller, M. C., Lamb, F. K., & Psaltis, D. 1998, ApJ, 508, 791
Muno, M. P., Galloway, D. K. Chakrabarty, D., & Psaltis, D. 2002a, ApJ, 580, 1048
Muno, M. P., Özel, F., & Chakrabarty, D. 2002b, ApJ, 581, 550
Nath, N. R., Strohmayer, T. E., & Swank, J. H. 2002, ApJ, 564, 353
Page, D. 1995, ApJ, 442, 273
Pechenick, K. R., Ftaclas, C., & Cohen, J. M. 1983, ApJ, 274, 846
Press, W. H., Teukolsky, S. A., Vetterling, W. T. & Flannery, B. P. 1992, Numerical Recipes in C, 2nd Ed. (Cambridge: Cambridge University Press)
Radhakrishnan, V. & Srinivasan, G. 1982, Curr. Sci., 51, 1096
Sazonov, S. Y. & Sunyaev, R. A. 2001, A&A, 373, 241
Strohmayer, T. E. 2001, Adv. Space. Res., 28, 511
Strohmayer, T. E., Jahoda, K., Giles, A. B., & Lee, U. 1997, ApJ, 486, 355
Strohmayer, T. E. & Markwardt, C. B. 1999, ApJ, 516, L81
Strohmayer, T. E. & Markwardt, C. B. 2002, ApJ, submitted
Strohmayer, T. E., Zhang, W., Swank, J. H., & Lapidus, I. 1998b, ApJ, 503, L147
Strohmayer, T. E., Zhang, W., Swank, J. H., White, N. E., & Lapidus, I. 1998a, ApJ, 498, L135
Strohmayer, T. E., Zhang, W., Swank, J. H., Smale, A., Titarchuk, L., Day, C., & Lee, U. 1996, ApJ, 469, L9
Vaughan, B. A. et al. 1994, ApJ, 435, 362
Weinberg, N., Miller, M. C., & Lamb, D. Q. 2001, ApJ, 546, 1098

TABLE 1
RXTE/PCA CHANNEL-TO-ENERGY CONVERSION

Channel	Energy (keV) during Epoch 3	4	5
5	2.3	2.5	2.5
13	5.1	5.9	5.7
18	6.9	8.0	7.8
28	10	12	12
36	13	16	15
53	20	23	22

Note. — Boundaries for the seven energy intervals used in this paper, where the first interval is 0-5, and the last 53-255. See text for explanation of gain epochs.

Table 2
Summed Profiles of Oscillations

Source	Frequency (Hz)	Gain Epoch	No. Osc.	Total Counts	Bkgd. Counts
4U 1636−536	581	3	6	312814	46871
		4	5	219356	23767
		5	4	317775	39453
MXB 1659−298	567	4	3	27782	5761
4U 1702−429	329	3	7	547076	47668
		5	1	38883	5236
4U 1728−34	363	3	12	552565	70491
		4	6	291955	69510
KS 1731−260	321	3	4	249986	43025
Aql X-1	549	3	2	120894	5754
		4	1	133784	6736

Table 3
Amplitudes of Burst Oscillations as a Function of Energy

Source	Gain Epoch	Constant χ^2_ν	Linear Trend Slope [% keV^{-1}]	χ^2_ν
4U 1636−536	3	17	0.448(6)	0.9
	4	16	0.390(6)	1.1
	5	108	0.889(5)	5.4
MXB 1659−298	4	5.9	0.777(18)	0.7
4U 1702−429	3	48	0.523(3)	2.2
4U 1728−34	3	11	0.263(4)	1.6
	4	126	0.582(6)	2.0
KS 1731−260	3	14	0.462(6)	0.9
Aql X-1	3	8.8	0.447(8)	0.2

Note. — 5 channels were used in computing χ^2_ν, so there were 4 degrees of freedom assuming a constant amplitude, and 3 assuming a linear trend.

Table 4
Phases of Burst Oscillations as a Function of Energy

Source	Gain Epoch	Constant χ^2_ν	Linear Trend Slope [10^{-3}cycles keV^{-1}]	χ^2_ν
4U 1636−536	3	1.0	1.92(14)	0.6
	4	2.0	3.57(14)	0.7
	5	0.8	−0.40(8)	0.9
MXB 1659−298	4	2.6	7.74(25)	0.3
4U 1702−429	3	2.4	1.97(10)	1.6
4U 1728−34	3	4.5	3.41(13)	3.5
	4	3.5	4.31(11)	0.8
KS 1731−260	3	0.5	1.58(18)	0.2
Aql X-1	3	0.8	3.04(29)	0.5

Note. — 5 channels were used in computing χ^2_ν, so there were 4 degrees of freedom assuming a constant amplitude, and 3 assuming a linear trend.